EFFICIENT 3-DIMENSIONAL MODEL RECONSTRUCTION BASED ON MARKER ENCODED FRINGE PROJECTION PROFILOMETRY

B. Budianto and Daniel P.K. Lun
Centre for Signal Processing, Department of Electronic and Information Engineering
The Hong Kong Polytechnic University, Hong Kong
budianto@ieee.org, enpklun@polyu.edu.hk

ABSTRACT

This paper presents a novel marker encoded fringe projection profilometry (FPP) scheme for efficient 3-dimensional (3D) model reconstruction. Traditional FPP schemes often have large error when reconstructing 3D model of objects with abruptly changing height profile. In the proposed scheme, markers are encoded in the projected fringe pattern to resolve the ambiguities in the fringe images due to that problem. Using the analytic complex wavelet, the marker cue information can be extracted from the fringe image, and is used to restore the order of the fringes. A series of simulations and experiments have been carried out to verify the proposed scheme. Experimental results show that the proposed method can accurately reconstruct the 3D model of objects with abruptly changing height profile. It is superior to the traditional FPP methods and facilitates real time 3D measurement for color object using only a single fringe image.

***Index Terms*—** Fringe projection profilometry, 3D model reconstruction.

1. INTRODUCTION

Due to the relatively low cost and high efficiency, structured light systems (SLS) are popularly used nowadays in applications that require the reconstruction of the 3-dimensional (3D) model of objects. In such systems, light patterns are projected onto the target object and the 3D model of the object can be reconstructed based on the displacement of the patterns as shown on the object surface. One of the popular approaches is the fringe projection profilometry (FPP). For FPP, the deformed fringe pattern as shown on the object surface can be mathematically modeled as follows:

$$g(x,y) = a(x,y) + b(x,y)\cos\left[\varphi_y(x)\right] \tag{1}$$

where $\varphi_y(x) = 2\pi f_0 x + \phi_y(x)$; $a(x,y)$ is the bias caused by the surface illumination of the object in x and y directions; $b(x,y)$ and f_0 are the local amplitude and the carrier frequency of the fringe pattern, respectively. In (1), $\phi_y(x)$ is an important parameter that has a direct relationship with the object height. If $\phi_y(x)$ is known, the 3D model of the object can be readily reconstructed.

To extract $\phi_y(x)$ from the fringe image *g(x,y)*, two classes of approaches are commonly employed: temporal phase shifting [1-6] and frequency multiplexing [7-11]. The phase shifting approaches use several shifted fringe patterns to cancel out the effects of the ambient light and reflection of the background before reconstructing the 3D model of the object. Such approaches are also called the phase shifted profilometry (PSP). While PSP can give good performance, problem arises if the target object is moving during the reconstruction process. Indeed any slight movement of the object during the process can lead to disastrous effect to the reconstructed 3D model. In contrast, the frequency multiplexing approaches can isolate the phase information in the frequency domain using only a single fringe pattern. Examples of such approaches include Fourier transform profilometry (FTP) [7], wavelet transform profilometry [12-13], FTP using the dual tree complex wavelet transform (DTCWT) [11], and FTP with color code[14-15].

However for a typical fringe analysis process using either class of approaches, the desired ϕ often cannot be obtained. Due to the ambiguity in (1) that the cosine function will give the same value for all phase angles φ separated by a multiple of 2π, current fringe analysis processes can only give the wrapped phase $\hat{\varphi}$ with value limited from $-\pi$ *to* π, where,

$$\varphi_y(x) = \hat{\varphi}_y(x) + k_y(x)2\pi \tag{2}$$

In (2), $k_y(x)$ is the so-called phase order that determines the number of 2π jumps required to unwrap the wrapped phase. Assuming that all wrapped phase information is available and there is no phase jump in φ (i.e. phase change larger than 2π), the desired phase φ can be recovered using different phase unwrapping methods (e.g. [16]). They indeed have been a de facto procedure in existing FPP systems. However, it is noticed that when working in practical environments, the acquired fringe images often have phase jumps (caused by sharp changes in object height) or some of the wrapped phase information is missing (caused by noise or other artifacts in the fringe image). Most phase unwrapping algorithms fail in this case to produce satisfactory result.

In this paper, we propose a new marker coding and detection algorithm. First, we embed markers that indicate

978-1-4799-2893-4/14/$31.00 ©2014 IEEE

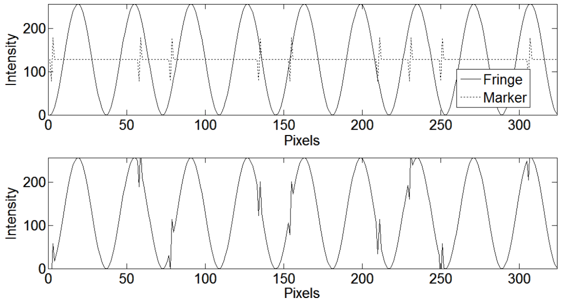

Fig. 1. The original sinusoidal fringe pattern and the marker codes (top). Marker encoded fringe pattern with eight periods and eight markers placed at different phase angles of each period (bottom).

the sequence number of each cosine period into the fringe pattern and project the fringe pattern onto an object. A snapshot of the fringe pattern with markers is shown in Fig.2. Second, the fringe image is captured and, using the Dual Tree Complex Wavelet Transform (DTCWT)[17], the markers are detected and extracted from the fringe image. Finally the phase order is estimated from the detected markers and is applied to the phase unwrapping process to obtain the absolute phase information. We can then make use of the phase information to reconstruct the 3D model of the object. A series of simulations and experiments using real objects are carried out to evaluate the proposed algorithm. For simple objects, the proposed algorithm can reconstruct 3D model with a similar quality as the traditional methods but at a much higher speed. It is due to the simplified phase unwrapping process resulted from the introduction of markers in the fringe pattern. For objects that have sharp changes in height, the proposed algorithm can accurately reconstruct the object height while the traditional approaches will fail since they use the conventional phase unwrapping methods.

2. PROPOSED MARKER CODING SCHEME

As mentioned in Section I, the process of FPP is to estimate the phase information ϕ from a fringe image g as defined in (1). Based on ϕ, the 3D model of the object can be readily reconstructed. To obtain ϕ, it is shown in (1) that we need to obtain φ first. However traditional fringe analysis processes only return the wrapped phase $\hat{\varphi}$ with value lies on $(-\pi,\pi]$. The method for retrieving φ from $\hat{\varphi}$ has been well studied [18]. Many existing solutions for phase unwrapping are based on Itoh's analysis [21], which indicates that the desired phase φ can be recovered by integrating the wrapped phase differences. When applying to FPP, the unwrapping process can be written as follows:

$$\varphi_y(n) = \hat{\varphi}_y(0) + \sum_{x=1}^{m} \Delta\hat{\varphi}_y(x) \qquad (3)$$

where $\varphi_y(n)$ is the estimated absolute phase at position n, $\Delta\hat{\varphi}_y(x) = \hat{\varphi}_y(x) - \hat{\varphi}_y(x-1)$ and $-\pi < \Delta\hat{\varphi}_y(x) \le \pi$. However, (3) is valid only if $\Delta\hat{\varphi}_y(x)$ for all x is available. If for a particular point x' such that $\Delta\hat{\varphi}_y(x')$ is missing or obtained with error, the unwrapped $\varphi_y(x)$ will have error for all $x \ge x'$. Such situation is common in typical FPP setup.

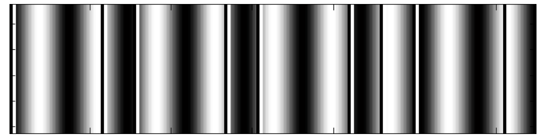

Fig. 2. A fringe pattern with markers located at different positions of different periods.

In fact even if some of the $\hat{\varphi}_y(x)$ are missing, we would still be able to retrieve $\varphi_y(x)$ from the remaining $\hat{\varphi}_y(x)$ by using (2) if the phase order $k_y(x)$ is known. In the proposed algorithm, markers are embedded into the projected fringe pattern in order to facilitate the estimation of the phase order from the fringe image. Given $g_y(x) \equiv g(x,y)$ for a specific y, the fringe image with marker embedded is defined as

$$p_y(x) = g_y(x) + m_y(x) \qquad (4)$$

where $m_y(x)$ is the marker sequence embedded into the fringe image. An example is shown in Fig.1. In the figure, the original sinusoidal fringe pattern (solid line) is added with impulses (dotted line) at different x. These impulses are the markers $m_y(x)$ and their positions with respect to the sinusoidal function indicate the sequence number of each sinusoidal period. Assume that every sinusoidal period has a size of T_o pixels, where T_o = 36 in our experiment. Assume also that every marker has a size of T_m pixels, where T_m = 4 in our experiment. Then we can have at most $N_m = T_o / T_m$ unique markers, assumed that T_o is an integer multiple of T_m. In our experiment, 9 unique markers are inserted into every 9 sinusoidal periods respectively. It means that the proposed encoding scheme can resolve the ambiguity due to the missing of at most 8 sinusoidal periods. To improve the performance in detection, particularly when the fringe image is noisy, the distance between any two neighboring markers should be maximized. More specifically, the marker sequence $m_y(x)$ is constructed using the following method. Assume that initially $m_y(x) = 0$ for all x, and N_m is an odd number. Then,

$$\begin{aligned} m_y(x+x') &\Leftarrow m_y(x+x') + f(x') \\ &\text{if } \operatorname{mod}\left(\left(\frac{x - \operatorname{mod}(x,T_o)}{2N_m/(N_m+1)}\right) - x, T_o\right) = 0 \end{aligned} \qquad (5)$$

for all x. In (5), f is the marker function, which is indeed the differentiation of a delta function. The index $x' \in \{0,1,\cdots,T_m-1\}$. The resulting marker encoded fringe pattern can be seen as in Fig. 2. In the figure, the thick black and white columns are the sinusoidal fringe pattern. The sharp black and white lines are the markers added to the fringe pattern. It should be noted that the positions of the markers with respect to the sinusoidal function are different. For every nine sinusoidal periods, markers are added, based on (5), at phase angles $\{0,5\theta,1\theta,6\theta,2\theta,7\theta,3\theta,8\theta,4\theta\}$,

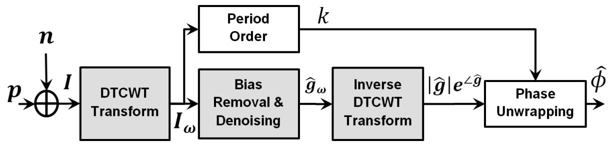

Fig. 3. Proposed Algorithm with DTCWT composition

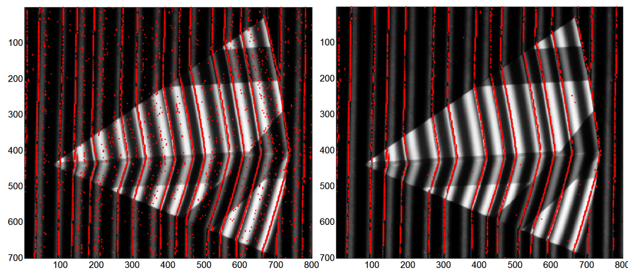

(a) (b)

Fig. 4. Marker detection using the maxima of the complex wavelet coefficients only (a) and after refinement (b)

respectively, where $\theta = 2\pi/9$. It is seen that for any 2 neighboring markers, they are separated by at least 4θ. Maximizing the distance of neighboring markers is important to the later marker detection process.

3. PROPOSED PHASE ORDER DETECTION ALGORITHM

The proposed marker detection algorithm is depicted as in Fig.3. In this paper, we focus on the Period Order Estimation block, which is responsible for detecting the markers from the fringe image and using them in the estimation of the phase order. Following the approach in [19], the DTCWT is used for removing the bias in the fringe image. At the same time, the 1st and 2nd level DTCWT coefficients that contain the marker information are fed to the Period Order Estimation block. The marker cue information Q is then obtained based on the DTCWT coefficients using the following formulation:

$$Q = \sum_{j=i}^{2} \Gamma_j \left(\alpha^j \left[\sum_{m=\{45^\circ,\,75^\circ,\,105^\circ,\,135^\circ\}} |d(j,m)| \right]^{\beta} \right) \qquad (6)$$

where $|d(j,m)|$ is the magnitude of the complex wavelet coefficients at level j and orientation subband m; parameter α and β are used to control the contribution of wavelet coefficients to the marker cue function; and $\Gamma_j(\cdot)$ is the interpolation function (e.g., bilinear interpolation) applied to the accumulation results of each level such that they have the same size as the original fringe image. Note that only some of the subbands are selected in the accumulation process since not all subbands contain significant marker information. Due to the shift invariance property of the DTCWT, the markers, which are indeed the discontinuities in the fringe image, will generate strong wavelet coefficients at the corresponding positions in the transform domain. Hence basically the positions of the maxima in Q are the positions of the markers in the fringe image. However, due to noise and other artifacts of the fringe image, many of the maxima of Q are not due to the markers. To remove the outlier, we use a 2-D rectangular mask centered at every maximum of Q and compute the variance σ of all

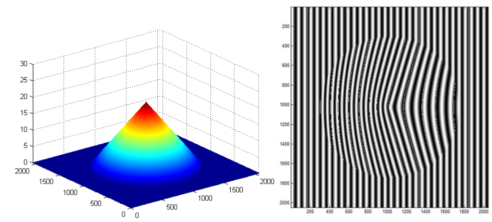

(a) (b)

Fig. 5. The object used in simulation, (a) A 3D cone (ground truth), (b) The deformed fringe image with markers added

coefficients of Q covered by this mask. Then a maximum is considered as introducing by a marker if the corresponding variance σ is greater than a threshold. A marker map is thus generated that indicates the position of the markers in the fringe image. Fig. 4 shows an example of the marker map (red lines or dots). It is seen that in Fig. 4a that the marker map using directly the maxima in Q has a lot of outliers. After the refinement process as mentioned above, a more accurate marker map can be obtained as shown in Fig. 4b.

We then make use of the detected markers to assist the phase unwrapping process. First, the flood fill algorithm [16] is used to find the regions in the fringe image in which the phase difference is bounded by 2π, i.e. in our case, one sinusoidal period. Let R_j be such region and j is the region index. Note that within the region R_j, there should be no phase wrapping hence it has the same phase order number k_j. As mentioned above, $k_j \in \{1 \ldots N_m\}$ which means that there can only be N_m possible values for k. An exhaustive search is thus carried out to determine k_j based on the markers detected in the region R_j as follows:

$$k_j = \min_i \frac{1}{N_j} \sum_y \left(\varphi_y\left(x_m^j\right) - \varphi_{ref}(i) \right) \qquad (7)$$

In (7), $\varphi_y\left(x_m^j\right)$ is the phase angle at position $\{x_m^j, y\}$ where a marker of this region R_j on row y is found. φ_{ref} are the N_m possible phase angles; and N_j is the total number of markers that can be detected in region R_j. (7) allows the estimation of the phase order k even when some of the markers are missing in a particular region, as can be seen in Fig. 4, due to sharp change in object height, noise or other artifacts in the fringe image, etc. Based on the phase order k, phase unwrapping can be easily achieved using (2). And the 3-D model of the object can be readily reconstructed.

4. SIMULATIONS AND EXPERIMENT RESULTS

A series of simulation and experiments were performed to evaluate the accuracy and the computation efficiency of the proposal algorithm. The first simulation was performed by applying the proposed algorithm to a computer generated fringe image of a cone shape object, which serves as the ground truth to facilitate the evaluation process. Fig 5a and 5b shows the cone shape object and the fringe image with markers respectively. To mimic the practical working environment, white Gaussian noise with noise variance σ = 1.0 is added to the fringe image. The simulation was

Table 1. Simulation results comparing with WFF+Goldstein in terms of execution time and SNR

Methods	window size	Time (sec)	SNR (db)
WFF+Goldstein	8	59.197	31.247
WFF+Goldstein	16	61.398	31.803
WFF+Goldstein	32	77.426	31.881
WFF+Goldstein	64	77.714	22.123
Proposed algorithm	-	5.644	32.175

realized by MATLAB and executed with a PC running at 3.4 GHz. The test fringe image has a resolution of 2048×2048. We compare the proposed algorithm with a traditional approach, the Window Fourier Filtering (WFF) method [20] with the Goldstein phase unwrapping algorithm [16] implemented also by MATLAB. Table 1 shows the comparison results in terms of execution speed and SNR. As shown in the table, the proposed algorithm is faster by approximately 10 times than the WFF+Goldstein method with similar, if not better, SNR. The result shows that for normal objects (without sharp change in height), the proposed algorithm can reduce the computational complexity while achieving a similar quality. It is due to the new marker map which greatly simplifies the phase unwrapping process.

To understand the actual performance of the proposed algorithm in practical applications, we implemented the proposed algorithm with an FPP hardware setup, which contains a DLP projector and a digital SLR camera (Canon D400). The camera has a 22.2 x 14.8mm CMOS sensor and a 17-50mm lens. It is connected to a conventional computer with a 3.4GHz CPU and 16GB RAM for image processing. The contrast ratio of the projector is 2000:1 and it can give a light output of 3300ANSI lumens. Both devices are placed 700mm – 1200mm from the target object.

In our experiment, a marker encoded fringe pattern with resolution of 1024×1280 is generated and projected onto the target objects including a paper plane, boxes and a book (Fig. 6a and 6b). The fringe pattern consists of 40 sinusoids in x-direction; each has a length of 36 pixels. A marker is embedded to each sinusoid with 4 pixels width. There are 9 unique markers and repeated in every 9 sinusoids. We compare the proposed algorithm with the conventional unwrapping method, the Goldstein algorithm [16], particularly in the situation that there are phase jumps in the fringe image. As shown in Fig. 6a and 6b, we use objects with sharp change in height (two small boxes in Fig. 6a and the book in Fig. 6b). These objects will introduce phase jumps in the fringe image. The comparison results are depicted in Fig. 6e to Fig. 6h. While the paper plane is correctly reconstructed using both approaches, the conventional method incorrectly reconstructs the boxes and the book. The proposed method does not suffer from the same problem because the phase order information is obtained from the detected marker map.

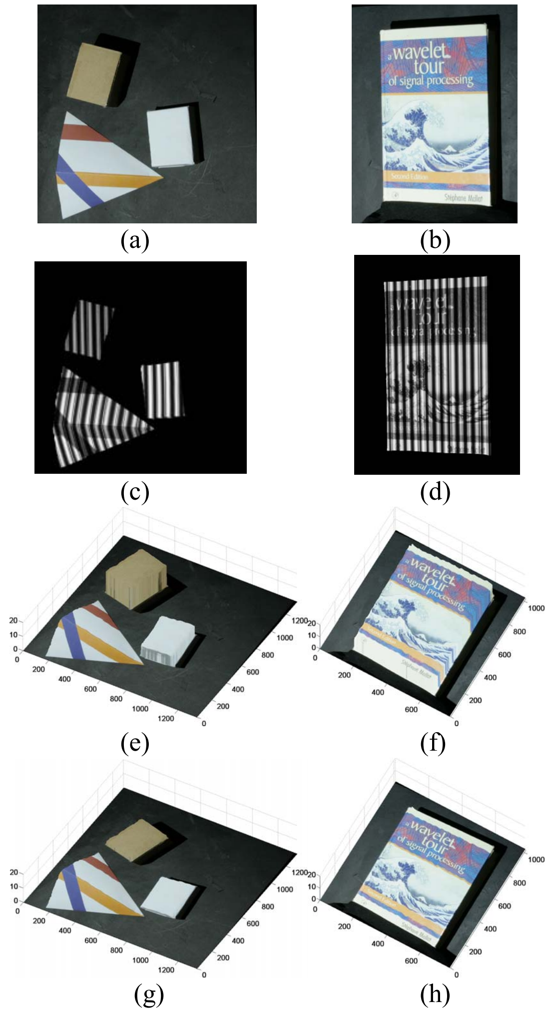

Fig. 6. Comparison of the proposed algorithm and the traditional phase unwrapping method. (a)-(b) Texture images; (c)-(d) fringe images; (e)-(f) results of the proposed algorithm; and (g)-(h) results of the traditional Goldstein method.

5. CONCLUSION

This paper proposed a new Fringe Projection Profilometry (FPP) scheme using a novel marker encoded fringe pattern for phase order estimation. The markers are indeed impulses embedded in the fringe pattern which can be extracted using the wavelet transform. With the markers, the phase order information can be estimated accurately and parsimoniously. Our simulation results show that the proposed algorithm can simplify the phase unwrapping process. Besides, the proposed algorithm can recover the height information correctly for objects with sharp change in height.

6. ACKNOWLEDGMENT

The work described in this paper was fully supported by the Hong Kong Polytechnic University (grant no. G-YL76).

7. REFERENCES

[1] Y. Wang, K. Liu, Q. Hao, D. L. Lau, and L. G. Hassebrook, “Period Coded Phase Shifting Strategy for Real-time 3-D Structured Light Illumination,” *Image Processing, IEEE Transactions on*, vol. 20, no. 11, pp. 3001–3013, 2011.

[2] T.-W. Hui and G. K.-H. Pang, “3-D Measurement of Solder Paste Using Two-Step Phase Shift Profilometry,” *Electronics Packaging Manufacturing, IEEE Transactions on*, vol. 31, no. 4, pp. 306–315, 2008.

[3] Y. Wang, K. Liu, Q. Hao, X. Wang, D. L. Lau, and L. G. Hassebrook, “Robust Active Stereo Vision Using Kullback-Leibler Divergence,” *Pattern Analysis and Machine Intelligence, IEEE Transactions on*, vol. 34, no. 3. pp. 548–563, 2012.

[4] S. Zhang and S.-T. Yau, “High-resolution, real-time 3D absolute coordinate measurement based on a phase-shifting method,” *Opt. Express*, vol. 14, no. 7, p. 2644, Apr. 2006.

[5] P. S. Huang and S. Zhang, “Fast three-step phase-shifting algorithm,” *Appl. Opt.*, vol. 45, no. 21, pp. 5086–5091, Jul. 2006.

[6] R. R. Garcia and A. Zakhor, “Consistent Stereo-Assisted Absolute Phase Unwrapping Methods for Structured Light Systems,” *Selected Topics in Signal Processing, IEEE Journal of*, vol. 6, no. 5, pp. 411–424, 2012.

[7] M. Takeda and K. Mutoh, “Fourier transform profilometry for the automatic measurement of 3-D object shapes,” *Appl. Opt.*, vol. 22, no. 24, pp. 3977–3982, 1983.

[8] T.-C. Hsung, D. P. Lun, and W. W. L. Ng, “Zero spectrum removal using joint bilateral filter for Fourier transform profilometry,” *Visual Communications and Image Processing (VCIP), 2011 IEEE*, pp. 1–4, 2011.

[9] A. Z. Abid, M. A. Gdeisat, D. R. Burton, M. J. Lalor, and F. Lilley, “Spatial fringe pattern analysis using the two-dimensional continuous wavelet transform employing a cost function,” *Appl. Opt.*, vol. 46, no. 24, p. 6120, Aug. 2007.

[10] C. Quan, C. J. Tay, and L. Chen, “Fringe-density estimation by continuous wavelet transform,” *Appl. Opt.*, vol. 44, no. 12, pp. 2359–2365, 2005.

[11] T.-C. Hsung, D. Pak-Kong Lun, and W. W. L. Ng, “Efficient fringe image enhancement based on dual-tree complex wavelet transform,” *Appl. Opt*, vol. 50, no. 21, pp. 3973–3986, 2011.

[12] M. A. Gdeisat, D. R. Burton, and M. J. Lalor, “Spatial carrier fringe pattern demodulation by use of a two-dimensional continuous wavelet transform,” *Appl. Opt.*, vol. 45, no. 34, pp. 8722–8732, Dec. 2006.

[13] D. Ali, Ã. Serhat, and F. N. Ecevit, “Continuous wavelet transform analysis of projected fringe patterns,” *Measurement Science and Technology*, vol. 15, no. 9, p. 1768, 2004.

[14] S. Fernandez and J. Salvi, “A novel Structured Light method for one-shot dense reconstruction,” *Image Processing (ICIP), 2012 19th IEEE International Conference on*. pp. 9–12, 2012.

[15] Y. Wang, S. Yang, and X. Gou, “Modified Fourier transform method for 3D profile measurement without phase unwrapping,” *Opt. Lett.*, vol. 35, no. 5, p. 790, Feb. 2010.

[16] D. C. G. and M. D. Pritt, *Two-dimensional phase unwrapping□: theory, algorithms, and software*. John Wiley & Sons, 1998.

[17] I. W. Selesnick, R. G. Baraniuk, and N. C. Kingsbury, “The dual-tree complex wavelet transform,” *Signal Processing Magazine, IEEE*, vol. 22, no. 6, pp. 123–151, 2005.

[18] K. Itoh, “Analysis of the phase unwrapping algorithm,” *Appl. Opt.*, vol. 21, no. 14, p. 2470, Jul. 1982.

[19] W. W.-L. Ng and D. P.-K. Lun, “Effective bias removal for fringe projection profilometry using the dual-tree complex wavelet transform,” *Appl. Opt.*, vol. 51, no. 24, pp. 5909–5916, Aug. 2012.

[20] Q. Kemao, “Windowed Fourier Transform for Fringe Pattern Analysis,” *Appl. Opt.*, vol. 43, no. 13, pp. 2695–2702, 2004.